

Higher order flutter analysis of doubly curved sandwich panels with variable thickness under aerothermoelastic loading

Mostafa livani^{*}, Keramat MalekzadehFard^a and Saeed Shokrollahi^b

Space Research Institute, MalekAshtar University of Technology, Tehran-Karaj Highway, Tehran, Iran

(Received February 16, 2016, Revised May 4, 2016, Accepted May 5, 2016)

Abstract. In this study, the supersonic panel flutter of doubly curved composite sandwich panels with variable thickness is considered under aerothermoelastic loading. Considering different radii of curvatures of the face sheets in this paper, the thickness of the core is a function of plane coordinates (x,y) , which is unique. For the first time in the current model, the continuity conditions of the transverse shear stress, transverse normal stress and transverse normal stress gradient at the layer interfaces, as well as the conditions of zero transverse shear stresses on the upper and lower surfaces of the sandwich panel are satisfied. The formulation is based on an enhanced higher order sandwich panel theory and the vertical displacement component of the face sheets is assumed as a quadratic one, while a cubic pattern is used for the in-plane displacement components of the face sheets and the all displacement components of the core. The formulation is based on the von Kármán nonlinear approximation, the one-dimensional Fourier equation of the heat conduction along the thickness direction, and the first-order piston theory. The equations of motion and boundary conditions are derived using the Hamilton principle and the results are validated by the latest results published in the literature.

Keywords: aerothermoelastic loading; doubly curved sandwich panels; variable thickness; enhanced higher order sandwich panel theory; piston theory

1. Introduction

Generally, the exteriors of the vehicles with supersonic speeds become exposed to severe aerodynamic loads as well as environmental temperatures. In a special case, a self-excited oscillation of the external skin can often occur when the velocity increases up to a certain point called the panel flutter speed. Panel flutter is known as a critical, multidisciplinary problem because it is induced by interactions among thermal loads, aerodynamic forces, and elastic restoring forces (Shin *et al.* 2009).

Wang (2003) investigated the flutter and buckling analyses of a fixed beam in the transverse direction under a static follower force. Navazi and Haddadpour (2007, 2011) studied the buckling analysis of functionally graded plates under thermal loading. Their formulation was based on the

^{*}Corresponding author, Ph.D. Student, E-mail: m_livani@mut.ac.ir

^aProfessor, E-mail: kmalekzadeh@mut.ac.ir

^bAssistant professor, E-mail: s_shokrollahi@mut.ac.ir

classical plate theory and the linear piston theory. Sohn and Kim (2009) investigated the thermal flutter analysis of functionally graded panels based on the first-order shear deformation theory, the von Kármán model and the first-order piston theory. The aerothermoelastic analysis of a curved skin panel was done by Abbas *et al.* (2011) based on the third-order piston theory aerodynamics, von Kármán model and Kirchhoff plate hypothesis. The flutter analysis of composite plates was done by Kuo (2011) based on the finite element method and linear piston theory. The effect of the variable fiber spacing on the response was considered. Shiau *et al.* (2012), Li and Song (2013) presented the aerothermoelastic analysis of composite laminated panels in supersonic flow based on the linear piston theory and Kirchhoff theory. Song and Li (2014) applied Reddy's third-order shear deformation theory and the piston theory to perform the nonlinear aeroelastic analysis and active flutter control of sandwich beams with pyramidal lattice core and the piezoelectric actuator/sensor pair. Yang *et al.* (2014) studied the aeroelastic analysis of single curved isotropic panels based on the modified piston theory. In their theory, only one transverse degree of freedom was considered. Zhao and Zhang (2014) applied the third-order piston theory, Reddy's third-order plate theory and von Kármán model to study the nonlinear dynamics analysis of composite laminated cantilever rectangular plates. Sankar *et al.* (2014, 2015) used the higher-order finite element method, zigzag function, and linear potential flow theory to study the panel flutter analysis of sandwich plates with carbon nanotube reinforced face sheets and a homogeneous core. Using the first order shear deformation theory and piston theory, Song and Li (2016) investigated aerothermoelastic analysis of composite sandwich panels.

Sandwich structures with laminated composite face sheets have historically been known to have the potential for high structural efficiency and have been extensively used in a variety of engineering applications including transportation, constructions and aerospace, in which strong, stiff and light components are required (MalekzadehFard and Livani 2015).

The higher-order sandwich panel theory was developed by Frostig *et al.* (1994, 2004), who considered two types of computational models for expressing the governing equations of the core. In the second Frostig's model, a polynomial description of the displacement fields was used for the core that was based on the displacement fields of the first Frostig's model. Their theory did not impose any restriction on the deformation distribution through the thickness of the core. To perform the buckling analysis of cylindrical and conical sandwich panels, Zhong and Reimerdes (2007) utilized the Kirchhoff-Love theory for the face sheets and neglected in-plane extensional and shear stiffnesses of the core. The thermoelastic buckling analysis of FG truncated conical shells was done by Naj *et al.* (2008) based on the first-order shell theory and Sanders nonlinear kinematics equations. Rahmani *et al.* (2009) applied the classical shell theory and an elasticity theory for the face sheets and the core, respectively to study the free vibration analysis of an open single curved composite sandwich shell. Kheirikhah *et al.* (2012) applied the third-order plate theory for the face sheets and quadratic and cubic functions for the transverse and in-plane displacements of the core to examine the bending analysis of composite sandwich plates. They also satisfied the continuity conditions for transverse shear stresses at the interfaces and the conditions of zero transverse shear stresses on the upper and lower surfaces. Using the Differential Quadrature method and the first-order shear deformation theory, Moradi and Mansouri (2012) performed the thermal buckling analysis of rectangular composite laminated plates under a uniform temperature distribution. Satisfying shear stress free surface conditions, Fekrar *et al.* (2012) conducted the buckling analysis of hybrid functionally graded plates based on a four variable refined plate theory. In this theory, the transverse shear stresses varied parabolically across the thickness. Using a thirteen nodes triangular element, Rezaiee-Pajand *et al.* (2012)

performed the bending analysis of composite sandwich plates. Jalili *et al.* (2014) applied numerical and experimental methods for studying the buckling analysis of composite conical panels under dynamic external pressures. They also investigated the effect of geometrical imperfections of experimental specimens on the numerical results. The bending and free vibration analyses of doubly curved composite sandwich panels with simply supported and fully clamped boundary conditions were performed by Malekzadefard *et al.* (2014a, b). In their theory, the first-order shear deformation theory and a polynomial description of the displacement fields based on the second Frostig's model were used for the composite face sheets and core, respectively. Using the first-order shear deformation theory, the free vibration and buckling analyses of functionally graded sandwich plates were done by Nguyen *et al.* (2014a). Thai *et al.* (2014) and Nguyen *et al.* (2014b) studied the static, buckling and free vibration analyses of isotropic and functionally graded sandwich plates using the inverse first-order shear deformation theory and trigonometric shear deformation theory. Nguyen *et al.* (2015) applied a four unknown higher-order shear deformation theory to perform the bending, vibration and buckling analyses of functionally graded sandwich plates.

The literature survey demonstrated that the most of the studies have been performed on the composite sandwich panels with constant thickness and no research is available in the field of thick doubly curved sandwich panels with variable thickness. In this study, the supersonic flutter of doubly curved composite sandwich panels with variable thickness under aerothermoelastic loading is investigated based on a three-dimensional elasticity theory. Considering different radii curvatures of the face sheets in this paper, the thickness of the core is a function of the plane coordinates (x, y) , which is unique. As a result, this study is able to analyze a wide range of sandwich panel configurations. For the first time in the current model, continuity conditions of the transverse shear stress, transverse normal stress and transverse normal stress gradient at the layer interfaces as well as the conditions of zero transverse shear stress on the upper and lower surfaces of the sandwich panel are satisfied. The formulation is based on an enhanced higher order sandwich panel theory, the von Kármán model and first-order high Mach number approximation. The vertical displacement component of the face sheets is assumed as a quadratic one while a cubic pattern is used for the in-plane displacement components of the face sheets and all the displacement components of the core. Also, the transverse normal and shear strain and stress of the core and face sheets as well as their in-plane strain and stress are considered. The equations of motion and boundary conditions are derived using the Hamilton principle.

2. Theoretical formulation

Consider a doubly curved composite sandwich panel which is composed of two composite laminated face sheets. The sandwich is composed of three layers: the top and bottom face sheets and core layer. As shown in Fig. 1, the length and width of panel are a and b , respectively. The Cartesian coordinate system $(x_i, y_i, z_i, i=t,b,c)$ are also shown in Fig. 1, in which indices t, b and c refer to the top and bottom face sheets and core of the panel, respectively and the z coordinate of each layer is measured upward from its mid-plane. The face sheets are laminated composites that assumed to have uniform thickness and the thicknesses of the top and bottom face sheets are h_t and h_b , respectively. Curvature radii of the top and bottom face sheets and core in x - z and y - z planes are R_{tx}, R_{bx}, R_{cx} and R_{ty}, R_{by}, R_{cy} , respectively. The core is also assumed as soft orthotropic material that due to consideration of different radii curvatures of the face sheets has non-uniform thickness.

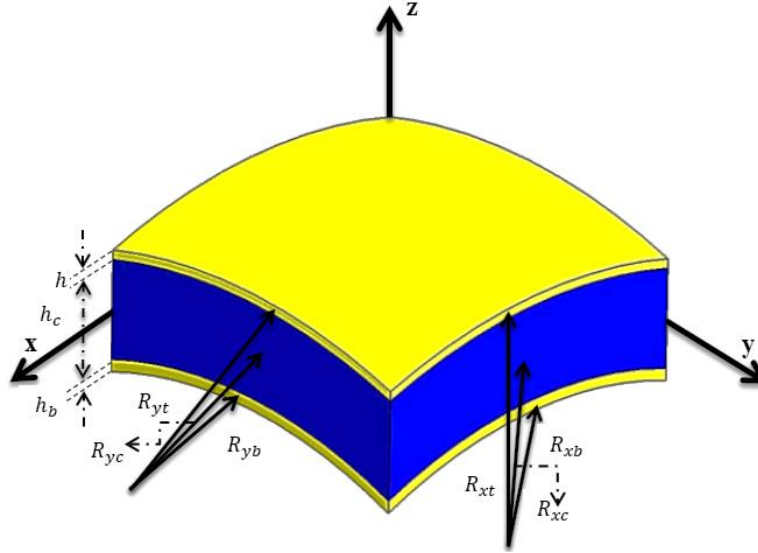


Fig. 1 A doubly curved sandwich panel with laminated face sheets

The thickness of the core is a function of the plane coordinates (x,y) .

The mid-surface equation of the panel with length of a and width of b and curvature radii R_x and R_y in x - z and y - z planes respectively is (Leissa and Kadi 1971)

$$z = -\frac{1}{2} \left(\frac{x^2}{R_x} + \frac{y^2}{R_y} \right) \quad (1)$$

where the origin of the coordinate is located in the center of the panel, then for the case that the origin of coordinate is located in the corner of the panel, Eq. (1) is to be in the following form

$$z = -\frac{(x-a/2)^2}{2R_x} - \frac{(y-b/2)^2}{2R_y} \quad (2)$$

then the relation of the upper and lower surfaces of the face sheets and core can be defined as follows

$$\begin{aligned} z_i^u(x, y) &= \frac{h_i}{2} - \frac{1}{2R_{xi}} \left(x - \frac{a}{2} \right)^2 - \frac{1}{2R_{yi}} \left(y - \frac{b}{2} \right)^2, \\ z_i^l(x, y) &= -\frac{h_i}{2} - \frac{1}{2R_{xi}} \left(x - \frac{a}{2} \right)^2 - \frac{1}{2R_{yi}} \left(y - \frac{b}{2} \right)^2; (i = t, b) \end{aligned} \quad (3)$$

$$z_c^u(x, y) = \frac{h_c^0}{2} - \frac{1}{2R_{xt}} \left(x - \frac{a}{2} \right)^2 - \frac{1}{2R_{yt}} \left(y - \frac{b}{2} \right)^2, \quad z_c^l(x, y) = -\frac{h_c^0}{2} - \frac{1}{2R_{xb}} \left(x - \frac{a}{2} \right)^2 - \frac{1}{2R_{yb}} \left(y - \frac{b}{2} \right)^2.$$

where h_c^0 is the thickness of the core in the center of the panel.

2.1 Kinematic relations

The displacement fields of the face sheets are based on the second Frostig's model (Frostig and Thomsen 2004) for the thick core, take a cubic pattern for the in-plane displacements and a quadratic one for the vertical ones and are read as

$$\begin{aligned} u_i(x, y, z_i, t) &= u_{0i}(x, y, t) + u_{1i}(x, y, r)z_i + u_{2i}(x, y, t)z_i^2 + u_{3i}(x, y, t)z_i^3, \\ v_i(x, y, z_i, t) &= v_{0i}(x, y, t) + v_{1i}(x, y, r)z_i + v_{2i}(x, y, t)z_i^2 + v_{3i}(x, y, t)z_i^3, \\ w_i(x, y, z_i, t) &= w_{0i}(x, y, t) + w_{1i}(x, y, r)z_i + w_{2i}(x, y, t)z_i^2 \quad ; \quad (i = t, b) \end{aligned} \quad (4)$$

where z_i is the vertical coordinate of each face-sheet ($i=t, b$) and is measured upward from the mid-plane of each face-sheet. The nonlinear von Kármán kinematic equations for the face sheets are as follows (Sankar *et al.* 2015)

$$\begin{aligned} \varepsilon_{xxi} &= \frac{\partial u_i}{\partial x} + \frac{w_i}{R_{xi}} + \frac{1}{2} \left(\frac{\partial w_i}{\partial x} \right)^2, \quad \varepsilon_{yyi} = \frac{\partial v_i}{\partial y} + \frac{w_i}{R_{yi}} + \frac{1}{2} \left(\frac{\partial w_i}{\partial y} \right)^2, \quad \varepsilon_{zzi} = \frac{\partial w_i}{\partial z_i} \quad ; \quad i = t, b \\ \gamma_{xyi} &= 2\varepsilon_{xyi} = \frac{\partial u_i}{\partial y} + \frac{\partial v_i}{\partial x}, \quad \gamma_{xzi} = 2\varepsilon_{xzi} = \frac{\partial u_i}{\partial z_i} + \left(\frac{\partial w_i}{\partial x} - \frac{u_i}{R_{xi}} \right), \quad \gamma_{yzi} = 2\varepsilon_{yzi} = \frac{\partial v_i}{\partial z_i} + \left(\frac{\partial w_i}{\partial y} - \frac{v_i}{R_{yi}} \right). \end{aligned} \quad (5)$$

Also, the all displacement fields of the core are a cubic polynomial functions as

$$\begin{aligned} u_c(x, y, z_c, t) &= u_{0c}(x, y, t) + u_{1c}(x, y, r)z_c + u_{2c}(x, y, t)z_c^2 + u_{3c}(x, y, t)z_c^3, \\ v_c(x, y, z_c, t) &= v_{0c}(x, y, t) + v_{1c}(x, y, r)z_c + v_{2c}(x, y, t)z_c^2 + v_{3c}(x, y, t)z_c^3, \\ w_c(x, y, z_c, t) &= w_{0c}(x, y, t) + w_{1c}(x, y, r)z_c + w_{2c}(x, y, t)z_c^2 + w_{3c}(x, y, t)z_c^3. \end{aligned} \quad (6)$$

Kinematic relations of the core for a doubly curved sandwich panel that are based on nonlinear von Kármán nonlinear strain approximation can be written as

$$\begin{aligned} \varepsilon_{xxc} &= \frac{1}{(1+z_c/R_{xc})} \left[\frac{\partial u_c}{\partial x} + \frac{w_c}{R_{xc}} + \frac{1}{2} \left(\frac{\partial w_c}{\partial x} \right)^2 \right], \quad \varepsilon_{yyc} = \frac{1}{(1+z_c/R_{yc})} \left[\frac{\partial v_c}{\partial y} + \frac{w_c}{R_{yc}} + \frac{1}{2} \left(\frac{\partial w_c}{\partial y} \right)^2 \right], \\ \varepsilon_{zxc} &= \frac{\partial w_c}{\partial z_c}, \quad \gamma_{xyc} = 2\varepsilon_{xyc} = \frac{1}{(1+z_c/R_{yc})} \frac{\partial u_c}{\partial y} + \frac{1}{(1+z_c/R_{xc})} \frac{\partial v_c}{\partial x}, \\ \gamma_{zxc} &= 2\varepsilon_{zxc} = \frac{\partial u_c}{\partial z_c} + \frac{1}{(1+z_c/R_{xc})} \left(\frac{\partial w_c}{\partial x} - \frac{u_c}{R_{xc}} \right), \quad \gamma_{zyc} = 2\varepsilon_{zyc} = \frac{\partial v_c}{\partial z_c} + \frac{1}{(1+z_c/R_{yc})} \left(\frac{\partial w_c}{\partial y} - \frac{v_c}{R_{yc}} \right). \end{aligned} \quad (7)$$

2.2 Thermal analysis

To obtain the steady state temperature distribution, the one-dimensional Fourier equation of the heat conduction in the thickness direction was solved, as follows

$$-\frac{d}{dz_i} \left(k_i \frac{dT_i}{dz_i} \right) = 0 \quad ; \quad i = t, c, b. \quad (8)$$

where k_i ($i=t, c, b$) is heat transfer coefficient. To solve the steady state temperature distribution

using Eq. (8), six boundary conditions were needed, as follows

$$\begin{aligned} T_t(z_t = z_t^u) &= T_u, & T_b(z_b = z_b^l) &= T_l, \\ T_t(z_t = z_t^l) &= T_c(z_c = z_c^u), & T_b(z_b = z_b^u) &= T_c(z_c = z_c^l), \\ k_t \frac{\partial T_t}{\partial z_t} \Big|_{z_t = z_t^l} &= k_c \frac{\partial T_c}{\partial z_c} \Big|_{z_c = z_c^u}, & k_b \frac{\partial T_b}{\partial z_b} \Big|_{z_b = z_b^u} &= k_c \frac{\partial T_c}{\partial z_c} \Big|_{z_c = z_c^l}. \end{aligned} \quad (9)$$

where T_u and T_l are the temperatures of the upper and lower surfaces of the sandwich panel, respectively. Now using Eqs. (8)-(9), equations of the steady state temperature distribution of the face sheets and core are obtained, as follows

$$T_t(z_t) = T_t^0 + z_t T_t^I, \quad T_c(z_c) = T_c^0 + z_c T_c^I, \quad T_b(z_b) = T_b^0 + z_b T_b^I. \quad (10)$$

where

$$\begin{aligned} T_t^0 &= T_u - \frac{(T_u - T_l) z_t^u(0,0)}{k_t k^*}, \quad T_t^I = \frac{T_u - T_l}{k_t k^*}, \quad T_c^0 = T_u - \left[\frac{z_c^u(0,0)}{k_c} + \frac{z_t^u(0,0) - z_t^l(0,0)}{k_t} \right] \frac{T_u - T_l}{k^*}, \\ T_c^I &= \frac{T_u - T_l}{k_c k^*}, \quad T_b^0 = T_l - \frac{(T_u - T_l) z_b^l(0,0)}{k_b k^*}, \quad T_b^I = \frac{T_u - T_l}{k_b k^*}. \end{aligned} \quad (11)$$

2.3 Compatibility conditions

The compatibility conditions in this paper were perfect bonding between the face sheets and core, continuity conditions of the transverse shear stresses, transverse normal stress and transverse normal stress gradient at the layer interfaces and the conditions of zero transverse shear stresses on the upper and lower surfaces of the sandwich panel. Note that to derive the compatibility conditions, the thermal effects were ignored. Assuming perfect bonding between the core and face sheets, the continuity conditions at the top and bottom face sheets-core interfaces are

$$\begin{aligned} u_t(z_t = z_t^l(x, y)) &= u_c(z_c = z_c^u(x, y)), & u_b(z_b = z_b^u(x, y)) &= u_c(z_c = z_c^l(x, y)), \\ v_t(z_t = z_t^l(x, y)) &= v_c(z_c = z_c^u(x, y)), & v_b(z_b = z_b^u(x, y)) &= v_c(z_c = z_c^l(x, y)), \\ w_t(z_t = z_t^l(x, y)) &= w_c(z_c = z_c^u(x, y)), & w_b(z_b = z_b^u(x, y)) &= w_c(z_c = z_c^l(x, y)). \end{aligned} \quad (12)$$

The continuity conditions of the transverse shear stresses at the face sheets and core interfaces are

$$\begin{aligned} \sigma_{xz t}(z_t = z_t^l(x, y)) &= \sigma_{z c}(z_c = z_c^u(x, y)), \quad \sigma_{yz t}(z_t = z_t^l(x, y)) = \sigma_{z c}(z_c = z_c^u(x, y)), \\ \sigma_{xz b}(z_b = z_b^u(x, y)) &= \sigma_{z c}(z_c = z_c^l(x, y)), \quad \sigma_{yz b}(z_b = z_b^u(x, y)) = \sigma_{z c}(z_c = z_c^l(x, y)). \end{aligned} \quad (13)$$

The continuity conditions of the transverse normal stress at the face sheets and core interfaces are

$$\sigma_{zz t}(z_t = z_t^l(x, y)) = \sigma_{z c}(z_c = z_c^u(x, y)), \quad \sigma_{zz b}(z_b = z_b^u(x, y)) = \sigma_{z c}(z_c = z_c^l(x, y)). \quad (14)$$

The continuity conditions of the transverse normal stress gradient at the face sheets and core interfaces are

$$\sigma_{z_t, z} (z_t = z_t^l(x, y)) = \sigma_{z_c, z} (z_c = z_c^u(x, y)), \sigma_{z_b, z} (z_b = z_b^u(x, y)) = \sigma_{z_c, z} (z_c = z_c^l(x, y)). \quad (15)$$

and finally, the conditions of zero transverse shear stresses on the upper surface of the top face sheet and the lower surface of the bottom face sheet are:

$$\sigma_{xz_t} (z_t = z_t^u(x, y)) = 0, \sigma_{yz_t} (z_t = z_t^u(x, y)) = 0, \sigma_{xz_b} (z_b = z_b^l(x, y)) = 0, \sigma_{yz_b} (z_b = z_b^l(x, y)) = 0. \quad (16)$$

2.4 Stress resultants

The stress resultants per unit length for the core can be defined as follow

$$\begin{aligned} \begin{Bmatrix} N_{xxc} \\ M_{xxc} \\ O_{xxc} \\ H_{xxc} \end{Bmatrix} &= \int_{z_c^l}^{z_c^u} \sigma_{xxc} \left(1 + \frac{z_c}{R_{yc}}\right) \begin{Bmatrix} 1 \\ z_c \\ z_c^2 \\ z_c^3 \end{Bmatrix} dz_c, \begin{Bmatrix} N_{yy c} \\ M_{yy c} \\ O_{yy c} \\ H_{yy c} \end{Bmatrix} = \int_{z_c^l}^{z_c^u} \sigma_{yy c} \left(1 + \frac{z_c}{R_{xc}}\right) \begin{Bmatrix} 1 \\ z_c \\ z_c^2 \\ z_c^3 \end{Bmatrix} dz_c, \begin{Bmatrix} N_{zzc} \\ M_{zzc} \\ O_{zzc} \end{Bmatrix} = \int_{z_c^l}^{z_c^u} \sigma_{zzc} \begin{Bmatrix} 1 \\ z_c \\ z_c^2 \end{Bmatrix} \left(1 + \frac{z_c}{R_{xc}}\right) \left(1 + \frac{z_c}{R_{yc}}\right) dz_c, \\ \begin{Bmatrix} N_{yxc} \\ M_{yxc} \\ O_{yxc} \\ H_{yxc} \end{Bmatrix} &= \int_{z_c^l}^{z_c^u} \tau_{yxc} \left(1 + \frac{z_c}{R_{xc}}\right) \begin{Bmatrix} 1 \\ z_c \\ z_c^2 \\ z_c^3 \end{Bmatrix} dz_c, \begin{Bmatrix} N_{xyc} \\ M_{xyc} \\ O_{xyc} \\ H_{xyc} \end{Bmatrix} = \int_{z_c^l}^{z_c^u} \tau_{xyc} \left(1 + \frac{z_c}{R_{yc}}\right) \begin{Bmatrix} 1 \\ z_c \\ z_c^2 \\ z_c^3 \end{Bmatrix} dz_c, \begin{Bmatrix} Q_{xzc} \\ S_{xzc} \\ T_{xzc} \end{Bmatrix} = \int_{z_c^l}^{z_c^u} \tau_{xzc} \left(1 + \frac{z_c}{R_{xc}}\right) \left(1 + \frac{z_c}{R_{yc}}\right) \begin{Bmatrix} 1 \\ z_c \\ z_c^2 \end{Bmatrix} dz_c, \quad (17) \\ \begin{Bmatrix} Q_{yzc} \\ S_{yzc} \\ T_{yzc} \end{Bmatrix} &= \int_{z_c^l}^{z_c^u} \tau_{yzc} \left(1 + \frac{z_c}{R_{xc}}\right) \left(1 + \frac{z_c}{R_{yc}}\right) \begin{Bmatrix} 1 \\ z_c \\ z_c^2 \end{Bmatrix} dz_c, \begin{Bmatrix} Q_{xzc}^* \\ S_{xzc}^* \\ T_{xzc}^* \\ V_{xzc}^* \end{Bmatrix} = \int_{z_c^l}^{z_c^u} \tau_{xzc} \left(1 + \frac{z_c}{R_{yc}}\right) \begin{Bmatrix} 1 \\ z_c \\ z_c^2 \\ z_c^3 \end{Bmatrix} dz_c, \begin{Bmatrix} Q_{yzc}^* \\ S_{yzc}^* \\ T_{yzc}^* \\ V_{yzc}^* \end{Bmatrix} = \int_{z_c^l}^{z_c^u} \tau_{yzc} \left(1 + \frac{z_c}{R_{xc}}\right) \begin{Bmatrix} 1 \\ z_c \\ z_c^2 \\ z_c^3 \end{Bmatrix} dz_c. \end{aligned}$$

Because the face sheets are thin ($\frac{z_i}{R_{xi}}, \frac{z_i}{R_{yi}} \ll 1, i = t, b$), $\frac{z_i}{R_{xi}}$ and $\frac{z_i}{R_{yi}}$ can be neglected, therefore, the stress resultants per unit length for the face sheets can be defined as follow

$$\begin{aligned} \begin{Bmatrix} N_{xxi} \\ M_{xxi} \\ O_{xxi} \\ H_{xxi} \end{Bmatrix} &= \int_{z_i^l}^{z_i^u} \sigma_{xxi} \begin{Bmatrix} 1 \\ z_i \\ z_i^2 \\ z_i^3 \end{Bmatrix} dz_i, \begin{Bmatrix} N_{yyi} \\ M_{yyi} \\ O_{yyi} \\ H_{yyi} \end{Bmatrix} = \int_{z_i^l}^{z_i^u} \sigma_{yyi} \begin{Bmatrix} 1 \\ z_i \\ z_i^2 \\ z_i^3 \end{Bmatrix} dz_i, \begin{Bmatrix} N_{zzi} \\ M_{zzi} \end{Bmatrix} = \int_{z_i^l}^{z_i^u} \sigma_{zzi} \begin{Bmatrix} 1 \\ z_i \end{Bmatrix} dz_i, \\ \begin{Bmatrix} N_{xyi} \\ M_{xyi} \\ O_{xyi} \\ H_{xyi} \end{Bmatrix} &= \int_{z_i^l}^{z_i^u} \tau_{xyi} \begin{Bmatrix} 1 \\ z_i \\ z_i^2 \\ z_i^3 \end{Bmatrix} dz_i, \begin{Bmatrix} Q_{xzi} \\ S_{xzi} \\ T_{xzi} \\ V_{xzi} \end{Bmatrix} = \int_{z_i^l}^{z_i^u} \tau_{xzi} \begin{Bmatrix} 1 \\ z_i \\ z_i^2 \\ z_i^3 \end{Bmatrix} dz_i, \begin{Bmatrix} Q_{yzi} \\ S_{yzi} \\ T_{yzi} \\ V_{yzi} \end{Bmatrix} = \int_{z_i^l}^{z_i^u} \tau_{yzi} \begin{Bmatrix} 1 \\ z_i \\ z_i^2 \\ z_i^3 \end{Bmatrix} dz_i. (i = t, b) \quad (18) \end{aligned}$$

2.5 Governing equations

The equilibrium equations for the face sheets and core are derived using the Hamilton principle

$$\int_0^t \delta L dt \equiv \int_0^t [\delta K - \delta U + \delta W_{ext}] dt = 0. \quad (19)$$

where δK , δU and δW_{ext} denote variation of kinetic energy, variation of strain energy and virtual work done by applied forces, respectively. Also, δ denotes the variation operator.

The first variation of the kinetic energy, upon assuming the homogeneous conditions for the displacement and velocity with respect to the time coordinate, can be written as follows

$$\begin{aligned} \delta K = & - \iint_A [(I_{0i}\ddot{u}_{0i} + I_{1i}\ddot{u}_{1i} + I_{2i}\ddot{u}_{2i} + I_{3i}\ddot{u}_{3i})\delta u_{0i} + (I_{1i}\ddot{u}_{0i} + I_{2i}\ddot{u}_{1i} + I_{3i}\ddot{u}_{2i})\delta u_{1i} + (I_{2i}\ddot{u}_{0i} + I_{3i}\ddot{u}_{1i})\delta u_{2i} + (I_{3i}\ddot{u}_{0i})\delta u_{3i} \\ & + (I_{0i}\ddot{v}_{0i} + I_{1i}\ddot{v}_{1i} + I_{2i}\ddot{v}_{2i} + I_{3i}\ddot{v}_{3i})\delta v_{0i} + (I_{1i}\ddot{v}_{0i} + I_{2i}\ddot{v}_{1i} + I_{3i}\ddot{v}_{2i})\delta v_{1i} + (I_{2i}\ddot{v}_{0i} + I_{3i}\ddot{v}_{1i})\delta v_{2i} + (I_{3i}\ddot{v}_{0i})\delta v_{3i} + \\ & (I_{0i}\ddot{w}_{0i} + I_{1i}\ddot{w}_{1i} + I_{2i}\ddot{w}_{2i})\delta w_{0i} + (I_{1i}\ddot{w}_{0i} + I_{2i}\ddot{w}_{1i} + I_{3i}\ddot{w}_{2i})\delta w_{1i} + (I_{2i}\ddot{w}_{0i} + I_{3i}\ddot{w}_{1i})\delta w_{2i}] dx dy \\ & - \iint_A [(I_{0c}\ddot{u}_{0c} + I_{1c}\ddot{u}_{1c} + I_{2c}\ddot{u}_{2c} + I_{3c}\ddot{u}_{3c})\delta u_{0c} + (I_{1c}\ddot{u}_{0c} + I_{2c}\ddot{u}_{1c} + I_{3c}\ddot{u}_{2c})\delta u_{1c} + (I_{2c}\ddot{u}_{0c} + I_{3c}\ddot{u}_{1c})\delta u_{2c} + (I_{3c}\ddot{u}_{0c})\delta u_{3c} \\ & + (I_{0c}\ddot{v}_{0c} + I_{1c}\ddot{v}_{1c} + I_{2c}\ddot{v}_{2c} + I_{3c}\ddot{v}_{3c})\delta v_{0c} + (I_{1c}\ddot{v}_{0c} + I_{2c}\ddot{v}_{1c} + I_{3c}\ddot{v}_{2c})\delta v_{1c} + (I_{2c}\ddot{v}_{0c} + I_{3c}\ddot{v}_{1c})\delta v_{2c} + (I_{3c}\ddot{v}_{0c})\delta v_{3c} + \\ & (I_{0c}\ddot{w}_{0c} + I_{1c}\ddot{w}_{1c} + I_{2c}\ddot{w}_{2c} + I_{3c}\ddot{w}_{3c})\delta w_{0c} + (I_{1c}\ddot{w}_{0c} + I_{2c}\ddot{w}_{1c} + I_{3c}\ddot{w}_{2c})\delta w_{1c} + (I_{2c}\ddot{w}_{0c} + I_{3c}\ddot{w}_{1c})\delta w_{2c} + (I_{3c}\ddot{w}_{0c})\delta w_{3c}] dx dy. \end{aligned} \quad (20)$$

where the moments of inertia are

$$I_{ni} = \int_{z_i^l}^{z_i^u} (z_i^n \rho_i) dz_i, I_{nc} = \int_{z_c^l}^{z_c^u} (z_c^n \rho_c) \left(1 + \frac{z_c}{R_{xc}}\right) \left(1 + \frac{z_c}{R_{yc}}\right) dz_c; (i = t, b \text{ \& } n = 0, 1, 2, 3) \quad (21)$$

The first variation of the strain energy for a doubly curved sandwich panel with variable thickness includes the top and bottom face sheets and the core is

$$\begin{aligned} \delta U = & \sum_{i=t,b} \left[\iiint (\sigma_{xxi} \delta \varepsilon_{xxi} + \sigma_{yyi} \delta \varepsilon_{yyi} + \sigma_{zxi} \delta \varepsilon_{zxi} + \tau_{xyi} \delta \gamma_{xyi} + \tau_{xzi} \delta \gamma_{xzi} + \tau_{yzi} \delta \gamma_{yzi}) dz_i dx_i dy_i \right] \\ & + \iiint (\sigma_{xxc} \delta \varepsilon_{xxc} + \sigma_{yyc} \delta \varepsilon_{yyc} + \sigma_{zxc} \delta \varepsilon_{zxc} + \tau_{xyc} \delta \gamma_{xyc} + \tau_{xzc} \delta \gamma_{xzc} + \tau_{yzc} \delta \gamma_{yzc}) \left(1 + \frac{z_c}{R_{xc}}\right) \left(1 + \frac{z_c}{R_{yc}}\right) dz_c dx_c dy_c. \end{aligned} \quad (22)$$

In addition, the six perfect bonding conditions at the layer interfaces, eight continuity conditions of the transverse shear stresses, transverse normal stress and transverse normal stress gradient at the layer interfaces and four conditions of zero transverse shear stresses on the upper and lower surfaces of the plate are fulfilled by using eighteen Lagrange multipliers.

The first variation of the external work of the sandwich panel under the aerodynamic, mechanical and thermal loads is as follows

$$\delta W_{ext} = \iint_{A_i} \Delta p \delta w_{0i} dx dy + \iint_{A_i} [N_{xxi}^m \delta u_{0i} + N_{yyi}^m \delta v_{0i}] dx dy; i = t, b, c \quad (23)$$

where N_{xxi}^m and N_{yyi}^m are the external mechanical loadings in the x and y directions, respectively. Also in Eq. (23), Δp is the aerodynamic pressure which is calculated by the first-

order piston theory that for the doubly curved sandwich panel with variable thickness can be defined as follows (Sankar *et al.* 2014)

$$p - p_\infty = -\beta_a \left(w_{0t} + w_{1t} z_t^u + w_{2t} (z_t^u)^2 + z_t^u \right)_{,x} - g_a \left(\dot{w}_{0t} + \dot{w}_{1t} z_t^u + \dot{w}_{2t} (z_t^u)^2 \right) \quad (24)$$

where

$$\beta_a = \frac{\rho_a V_\infty^2}{\sqrt{M_\infty^2 - 1}}, g_a = \beta_a \left(\frac{M_\infty^2 - 2}{M_\infty^2 - 1} \right) \frac{1}{V_\infty} \quad (25)$$

By substitution of Eq. (24) into Eq. (23), we have

$$\begin{aligned} \delta W_{ext} = \iint_{A_i} \left[\beta_a \left(w_{0t} + w_{1t} z_t^u + w_{2t} (z_t^u)^2 + z_t^u \right)_{,x} + g_a \left(\dot{w}_{0t} + \dot{w}_{1t} z_t^u + \dot{w}_{2t} (z_t^u)^2 \right) \right] \\ \left\{ \delta w_{0t} + z_t^u \delta w_{1t} + (z_t^u)^2 \delta w_{2t} \right\} dx dy + \iint_{A_i} \left[N_{xxi}^m \delta u_{0i} + N_{yyi}^m \delta v_{0i} \right] dx dy; i = t, b, c \end{aligned} \quad (26)$$

Also by substitution of Eqs. (20), (22) and (26) into Eq. (19), and then integration by parts, the governing equations and appropriate boundary conditions can be obtained. The simply supported B.Cs. for a doubly curved sandwich panel at the edges $x=0, a$ of the panel are obtained as follow

$$\begin{aligned} N_{xxt} = \bar{N}_{xxt}, M_{xxt} = \bar{M}_{xxt}, O_{xxt} = 0, H_{xxt} = 0, v_{0t} = 0, v_{1t} = 0, v_{2t} = 0, v_{3t} = 0, w_{0t} = 0, w_{1t} = 0, w_{2t} = 0, \\ N_{xxb} = \bar{N}_{xxb}, M_{xxb} = \bar{M}_{xxb}, O_{xxb} = 0, H_{xxb} = 0, v_{0b} = 0, v_{1b} = 0, v_{2b} = 0, v_{3b} = 0, w_{0b} = 0, w_{1b} = 0, w_{2b} = 0, \\ N_{xxc} = \bar{N}_{xxc}, M_{xxc} = \bar{M}_{xxc}, O_{xxc} = 0, H_{xxc} = 0, v_{0c} = 0, v_{1c} = 0, v_{2c} = 0, v_{3c} = 0, w_{0c} = 0, w_{1c} = 0, w_{2c} = 0, w_{3c} = 0. \end{aligned} \quad (27)$$

and at the edges $y = 0, b$ of the panel are obtained as follow

$$\begin{aligned} N_{yyt} = \bar{N}_{yyt}, M_{yyt} = \bar{M}_{yyt}, O_{yyt} = 0, H_{yyt} = 0, u_{0t} = 0, u_{1t} = 0, u_{2t} = 0, u_{3t} = 0, w_{0t} = 0, w_{1t} = 0, w_{2t} = 0, \\ N_{yyb} = \bar{N}_{yyb}, M_{yyb} = \bar{M}_{yyb}, O_{yyb} = 0, H_{yyb} = 0, u_{0b} = 0, u_{1b} = 0, u_{2b} = 0, u_{3b} = 0, w_{0b} = 0, w_{1b} = 0, w_{2b} = 0, \\ N_{yyc} = \bar{N}_{yyc}, M_{yyc} = \bar{M}_{yyc}, O_{yyc} = 0, H_{yyc} = 0, u_{0c} = 0, u_{1c} = 0, u_{2c} = 0, u_{3c} = 0, w_{0c} = 0, w_{1c} = 0, w_{2c} = 0, w_{3c} = 0. \end{aligned} \quad (28)$$

where \bar{N}_{xxi} and \bar{N}_{yyi} ($i = t, b$) are the external loads in the x and y directions and \bar{M}_{xxi} and \bar{M}_{yyi} ($i = t, b$) are the bending moment about the x and y directions and can be obtained as

$$\bar{N}_{xxi} = N_{xxi}^m + N_{xxi}^T, \bar{N}_{yyi} = N_{yyi}^m + N_{yyi}^T, \bar{M}_{xxi} = \bar{M}_{xxi}^T, \bar{M}_{yyi} = \bar{M}_{yyi}^T; i = t, b, c \quad (29)$$

where superscript m and T are used for the mechanical and thermal loadings, respectively and

$$\begin{aligned} \left(\begin{Bmatrix} N_{xxi}^T \\ N_{yyi}^T \end{Bmatrix}, \begin{Bmatrix} M_{xxi}^T \\ M_{yyi}^T \end{Bmatrix} \right) = \Delta T_i \sum_{k=1}^{N_i} \int_{z_i^k}^{z_i^{k+1}} \begin{bmatrix} \bar{Q}_{11} & \bar{Q}_{12} \\ \bar{Q}_{12} & \bar{Q}_{22} \end{bmatrix}^{(k)} \begin{Bmatrix} \alpha_{xx} \\ \alpha_{yy} \end{Bmatrix}^{(k)} (1, z_i) dz_i; i = t, b \\ \left(\begin{Bmatrix} N_{xxc}^T \\ N_{yyc}^T \end{Bmatrix}, \begin{Bmatrix} M_{xxc}^T \\ M_{yyc}^T \end{Bmatrix} \right) = \int_{z_c^l}^{z_c^u} \begin{bmatrix} Q_{11} & Q_{12} & Q_{13} \\ Q_{12} & Q_{22} & Q_{23} \end{bmatrix} \begin{Bmatrix} \alpha_{xx} \\ \alpha_{yy} \\ \alpha_{zz} \end{Bmatrix} \Delta T_c \left(1 + \frac{z_c}{R_{xc}} \right) \left(1 + \frac{z_c}{R_{yc}} \right) (1, z_c) dz_c. \end{aligned} \quad (30)$$

3. Analytical solution

In this section, the procedure of determining the dimensionless critical dynamic pressure of the doubly curved sandwich panel under aerothermoelastic loading is presented. To do that, the right-hand side of the governing equations should be removed. Also the in-plane inertia terms of the governing equations are neglected, since based on research given by Reddy (2004), the deformations in these directions are smaller than that in the transverse direction. The displacement fields based on double Fourier series for a doubly curved composite sandwich panel satisfying the simply supported boundary conditions (Eqs. (27)-(28)) are assumed to be in the following forms

$$\begin{bmatrix} u_{ij}(x, y, t) \\ v_{ij}(x, y, t) \\ w_{ij}(x, y, t) \\ u_{ic}(x, y, t) \\ v_{ic}(x, y, t) \\ w_{ic}(x, y, t) \end{bmatrix} = \sum_{n=1}^N \sum_{m=1}^M \begin{bmatrix} U_{ij}^{mn} \cos(\alpha_m x) \sin(\beta_n y) \\ V_{ij}^{mn} \sin(\alpha_m x) \cos(\beta_n y) \\ W_{ij}^{mn} \sin(\alpha_m x) \sin(\beta_n y) \\ U_{ic}^{mn} \cos(\alpha_m x) \sin(\beta_n y) \\ V_{ic}^{mn} \sin(\alpha_m x) \cos(\beta_n y) \\ W_{ic}^{mn} \sin(\alpha_m x) \sin(\beta_n y) \end{bmatrix} e^{\Omega t}, \quad (i=0,1,2,3), (l=0,1,2), (j=t,b) \quad (31)$$

where $U_{ij}^{mn}, V_{ij}^{mn}, W_{ij}^{mn}, U_{ic}^{mn}, V_{ic}^{mn}$ and W_{ic}^{mn} are Fourier coefficients and m and n are half wave numbers along the x and y directions, respectively and $\Omega = \alpha + i\omega$ that α and ω are damping ratio and frequency. Also the Lagrange multipliers can be expressed in the following forms

$$\begin{bmatrix} \chi_x^{jc}(x, y, t) \\ \chi_y^{jc}(x, y, t) \\ \chi_z^{jc}(x, y, t) \\ \chi_{xz}^j(x, y, t) \\ \chi_{yz}^j(x, y, t) \\ \chi_{xz}^{jc}(x, y, t) \\ \chi_{yz}^{jc}(x, y, t) \\ \chi_{zz}^{jc}(x, y, t) \\ \chi_{zz'}^{jc}(x, y, t) \end{bmatrix} = \sum_{n=1}^N \sum_{m=1}^M \begin{bmatrix} X_{jc}^{mn} \cos(\alpha_m x) \sin(\beta_n y) \\ Y_{jc}^{mn} \sin(\alpha_m x) \cos(\beta_n y) \\ Z_{jc}^{mn} \sin(\alpha_m x) \sin(\beta_n y) \\ XZ_j^{mn} \cos(\alpha_m x) \sin(\beta_n y) \\ YZ_j^{mn} \sin(\alpha_m x) \cos(\beta_n y) \\ XZ_{jc}^{mn} \cos(\alpha_m x) \sin(\beta_n y) \\ YZ_{jc}^{mn} \sin(\alpha_m x) \cos(\beta_n y) \\ ZZ_{jc}^{mn} \sin(\alpha_m x) \sin(\beta_n y) \\ ZZ_{jc}^{mn} \cos(\alpha_m x) \cos(\beta_n y) \end{bmatrix} e^{\Omega t}, \quad (j=t,b) \quad (32)$$

where $X_{jc}^{mn}, Y_{jc}^{mn}, Z_{jc}^{mn}, XZ_j^{mn}, YZ_j^{mn}, XZ_{jc}^{mn}, YZ_{jc}^{mn}, ZZ_{jc}^{mn}$, and ZZ_{jc}^{mn} are Fourier coefficients.

To obtain governing equations, the Galerkin method is used. In this method, the coordinate functions are similar to the weighted functions as follows

$$\int_0^a \int_0^b ([\bar{L}]\{\phi\})\{\psi\} dx dy = \{0\}. \quad (33)$$

where $[\bar{L}]$ is a matrix of differential operators and ϕ and ψ are shape functions and weighting functions that are

$$\begin{aligned} \{\phi\}^T = & \left\{ \bar{U}_{ij}^{mn} \cos(\alpha_m x) \sin(\beta_n y), \bar{V}_{ij}^{mn} \sin(\alpha_m x) \cos(\beta_n y), \bar{W}_{lj}^{mn} \sin(\alpha_m x) \sin(\beta_n y), \bar{U}_{ic}^{mn} \cos(\alpha_m x) \sin(\beta_n y), \right. \\ & \bar{V}_{ic}^{mn} \sin(\alpha_m x) \cos(\beta_n y), \bar{W}_{ic}^{mn} \sin(\alpha_m x) \sin(\beta_n y), \bar{X}_{jc}^{mn} \cos(\alpha_m x) \sin(\beta_n y), \bar{Y}_{jc}^{mn} \sin(\alpha_m x) \cos(\beta_n y), \\ & \bar{Z}_{jc}^{mn} \sin(\alpha_m x) \sin(\beta_n y), \bar{XZ}_j^{mn} \cos(\alpha_m x) \sin(\beta_n y), \bar{YZ}_j^{mn} \sin(\alpha_m x) \cos(\beta_n y), \bar{XZ}_{jc}^{mn} \cos(\alpha_m x) \sin(\beta_n y), \\ & \left. \bar{YZ}_{jc}^{mn} \sin(\alpha_m x) \cos(\beta_n y), \bar{ZZ}_{jc}^{mn} \sin(\alpha_m x) \sin(\beta_n y), \bar{ZZ}_{jc}^{mn} \cos(\alpha_m x) \cos(\beta_n y) \right\} (i=0,1,2,3), (l=0,1,2), (j=t,b) \end{aligned} \quad (34)$$

$$\begin{aligned} \{\psi\}^T = & \left\{ \cos(\alpha_m x) \sin(\beta_n y), \sin(\alpha_m x) \cos(\beta_n y), \sin(\alpha_m x) \sin(\beta_n y), \cos(\alpha_m x) \sin(\beta_n y), \sin(\alpha_m x) \cos(\beta_n y), \right. \\ & \sin(\alpha_m x) \sin(\beta_n y), \cos(\alpha_m x) \sin(\beta_n y), \sin(\alpha_m x) \cos(\beta_n y), \sin(\alpha_m x) \sin(\beta_n y), \cos(\alpha_m x) \sin(\beta_n y), \\ & \left. \sin(\alpha_m x) \cos(\beta_n y), \cos(\alpha_m x) \sin(\beta_n y), \sin(\alpha_m x) \cos(\beta_n y), \sin(\alpha_m x) \sin(\beta_n y), \cos(\alpha_m x) \cos(\beta_n y) \right\}. \end{aligned}$$

Now by substituting displacement field (Eqs. (31)-(32)) into the governing equations, and applying the Galerkin's procedure and collecting coefficients, the final governing equations can be expressed in the following forms

$$[M]\{\ddot{X}\} + [C]\{\dot{X}\} + [K]\{X\} = \{0\}. \quad (35)$$

where $[M]$, $[C]$ and $[K]$ are the mass, aerodynamic damping, and stiffness matrices, respectively.

Also, $\{X\}$ is the vector of unknown coefficients:

$$\begin{aligned} \{X\}^T = & \left\{ \bar{U}_{ij}^{mn}, \bar{V}_{ij}^{mn}, \bar{W}_{lj}^{mn}, \bar{U}_{ic}^{mn}, \bar{V}_{ic}^{mn}, \bar{W}_{ic}^{mn}, \bar{X}_{jc}^{mn}, \bar{Y}_{jc}^{mn}, \bar{Z}_{jc}^{mn}, \bar{XZ}_j^{mn}, \bar{YZ}_j^{mn}, \bar{XZ}_{jc}^{mn}, \bar{YZ}_{jc}^{mn}, \bar{ZZ}_{jc}^{mn}, \bar{ZZ}_{jc}^{mn} \right\}; \\ & (i=0,1,2,3), (l=0,1,2), (j=t,b) \end{aligned}$$

The final governing equations can be reduced to a standard eigenvalue problem by transferring to state-space as (Seresta 2007)

$$\begin{aligned} \begin{Bmatrix} \dot{X} \\ \ddot{X} \end{Bmatrix} = & \begin{bmatrix} [0] & [I] \\ -[M]^{-1}[K] & -[M]^{-1}[C] \end{bmatrix} \begin{Bmatrix} X \\ \dot{X} \end{Bmatrix} \end{aligned} \quad (36)$$

where $[I]$ is the identity matrix. By varying the flow speed, eigenvalue analysis of the state space equation is performed. The instability occurs when the real part of one of the eigenvalues becomes positive; the flow speed for which the damping ratio becomes zero is the linear flutter speed.

4. Results and discussions

To study the aerothermoelastic stability of doubly curved composite sandwich panel with variable thickness, a computer program is developed based on the governing equations. In this section, some examples are considered and the obtained results are validated and discussed. To validate the present results and to demonstrate its capability, some examples are presented and the results obtained from the present theory are compared with the theoretical and numerical results found in literature. The agreement between the results was quite good.

Example 1

In this example, the free vibration analysis of a flat composite sandwich panel with a foam core and composite face sheets (Table 1) and simply supported boundary conditions (S.S. B.C.s) is investigated.

Table 1 Material properties of a flat composite sandwich panel (Rahmani *et al.* 2010)

Foam core	$E_1 = E_2 = E_3 = 0.10363 \text{ GPa}, G_{12} = G_{13} = G_{23} = 0.05 \text{ GPa}, \nu = 0.32, \rho = 130 \text{ kg / m}^3.$
Composite face sheets	$E_1 = 24.51 \text{ GPa}, E_2 = 7.77 \text{ GPa}, G_{12} = G_{13} = 3.34 \text{ GPa}, G_{23} = 1.34 \text{ GPa},$ $\nu_{12} = \nu_{13} = 0.078, \nu_{23} = 0.49, \rho = 1800 \text{ Kg / m}^3.$

Table 2 Comparing dimensionless natural frequencies of a flat composite sandwich panel with cross ply lay up $\bar{\omega} = \omega a^2 (\rho_c / E_c)^{1/2} / h, h / a = 0.1, h_c / h = 0.88, [0/90/0/\text{Core}/0/90/0]$

Mode No.	Present model	1st model of Frostig	Error (%)	ANSYS	Error (%)	HSDT-ESL	Error (%)
1	14.05	14.27	1.6	14.74	4.9	15.28	8.8
2	25.88	26.31	1.7	26.83	3.7	28.69	10.9
3	27.04	27.04	1.7	27.53	3.5	30.01	12.9
4	34.32	34.95	1.8	35.60	3.7	38.86	13.2

Table 3 Material properties of a cylindrical composite sandwich panel

Foam core	$E_1 = E_2 = E_3 = 6.89 \text{ MPa}, G_{12} = G_{13} = G_{23} = 3.45 \text{ MPa}, \nu = 0.32, \rho = 94.195 \text{ Kg / m}^3.$
Composite face sheets	$E_1 = 131 \text{ GPa}, E_2 = E_3 = 10.34 \text{ GPa}, G_{12} = G_{13} = 6.895 \text{ GPa}, G_{23} = 6.205 \text{ GPa},$ $\nu_{12} = \nu_{13} = 0.22, \nu_{23} = 0.49, \rho = 1627 \text{ Kg / m}^3.$

In Table 2, the results obtained from the present theory (IHSAPT) are compared with those obtained from the first model of Frostig (Rahmani *et al.* 2010), the higher order equivalent single layer theory (HSDT-ESL) (Meunier and Shenoi 1999) and FE modeling in ANSYS code (Rahmani *et al.* 2010). The maximum difference between the present theory and the higher order equivalent single layer theory (HSDT-ESL) is 13.2 percent. Due to core flexibility in the current theory, the obtained natural frequencies from the current theory are lower than the natural frequencies obtained from the FSDT-ESL. Also, the present results are in good agreement with those obtained from finite element ANSYS software and the first model of Frostig.

Example 2

In this example, the free vibration analysis of a cylindrical composite sandwich panel with a foam core is investigated. Mechanical properties of the face sheets and core are given in Table 3. In the Table 4, dimensionless first natural frequency for thin ($h/b=0.01$) and thick ($h/b=0.01$) sandwich panels with three different radii to width ratios (R/b) are presented. In this table, the results of the present theory (IHSAPT) are compared with those obtained from the first Frostig's model, FE modeling in ANSYS code (Rahmani *et al.* 2010), first order shear deformation theory, and higher order equivalent single layer theory (Armenakas *et al.* 1969). As can be seen in Table 4, the current results are in good agreement with the first Frostig's model results. Table 4 also demonstrates that results of different theories for the thin sandwich panel are in better agreement than those for the thick sandwich panel.

Example 3

In this example, the free vibration analysis of a spherical composite sandwich panel with S.S. B.C.s is investigated. Mechanical properties of the sandwich structure are given in Table 3. In Table

Table 4 Comparing dimensionless fundamental natural frequency of the cylindrical sandwich panel ([0/90])

R/b	h/b	Dimensionless natural frequency (a/b=1)								
		Present model	Frostig's 1st model	Error (%)	ANSYS	Error (%)	HSDT-ESL	Error (%)	FSDT-ESL	Error (%)
1	0.01	62.5	63.27	1.2	64.62	3.4	64.64	3.4	64.80	3.7
	0.1	5.52	5.65	2.4	6.46	17.0	7.71	39.7	14.16	156.5
2	0.01	33.6	33.87	0.8	34.50	2.7	35.90	6.8	36.21	7.8
	0.1	2.9	2.96	2.1	3.71	27.9	5.82	100.7	14.026	383.7
3	0.01	24.01	24.17	0.7	24.81	3.3	26.69	11.2	27.12	13.0
	0.1	2.16	2.19	1.4	2.83	31.0	5.37	148.6	14.00	548.1

Table 5 Comparing dimensionless fundamental natural frequency of a spherical sandwich panel ([0/90])

R/a	h/a	0.1			0.01		
		Present model	HSAPT	Error (%)	Present model	HSAPT	Error (%)
1		11.214	12.316	9.8	119.201	123.633	3.7
2		5.986	6.726	12.4	63.887	65.906	3.2
3		4.490	4.737	5.5	44.141	45.274	2.6
4		3.514	3.772	7.3	32.548	34.998	7.5
5		2.977	3.222	8.3	28.213	28.967	2.7
10		2.182	2.283	4.6	17.844	17.909	0.3
20		1.881	1.978	5.2	13.759	13.800	0.3

Table 6 Material properties of a flat laminate panel (Ganapathi and Varadan 1995)

Face sheets	$E_1 = 68.948 \text{ GPa}, E_2 = E_3 = 6.895 \text{ GPa}, G_{12} = G_{13} = 2.275 \text{ GPa}, G_{23} = 1.034 \text{ GPa}, \nu_{12} = \nu_{13} = \nu_{23} = 0.3.$
-------------	---

5, the current results are compared with the higher order sandwich plate theory (HSAPT) presented by Biglari and Jafari (2010). As can be seen in Table 5, the results of the present method are in good agreement with those of HSAPT; but, there is a little difference between the current results and those for the thick panel ($h/a=0.1$). It is because the HSAPT model do not consider the transverse stresses in the face sheets and the in-plane stresses in the core and the current method can rather accurately model flexibility of the core.

Example 4

In this example, the panel flutter analysis of a flat composite panel with S.S. B.C.s is investigated. Mechanical properties of a laminate panel are given in Table 6. Lay-up sequences of the laminate panel are [0/90/0/90] and [-45/45/-45/45]. In Table 7, the critical dynamic pressure ($\bar{\lambda}_{cr}$) obtained from the present theory are compared with those obtained from Ganapathi and Varadan (1995) based on the Mindlin theory and those obtained from Sawyer (1977) based on the classical plate theory. As demonstrates in this table, the agreement between the results is good.

Example 5

In this example the effect of the radii curvatures ratio on the panel flutter of doubly curved

Table 7 Comparing the critical dynamic pressure for the laminated panel $\bar{\lambda}_{cr} = \frac{\rho_a V_\infty^2 a^3}{\sqrt{M_\infty^2 - 1} D_{11}(0)}$

a/b	a/h	[-45/45/-45/45]			[0/90/0/90]	
		Present model	Mindlin theory	Classical plate theory	Present model	Mindlin theory
1	10	151.5	160.60	-	39.2	44.75
	100	206.1	-	222.7	52.7	54.6
2	10	266.6	282.25	-	52.9	58.39
	100	645.9	684.06	-	136.3	141.88

Table 8 Mechanical and geometrical properties of a doubly curved composite sandwich panel

Foam core	$E_1 = E_2 = E_3 = 6.89 \text{ MPa}$, $G_{12} = G_{13} = G_{23} = 3.45 \text{ MPa}$, $\nu = 0.25$, $\rho = 130 \text{ kg/m}^3$.
Composite face sheets	$E_1 = 131 \text{ GPa}$, $E_2 = E_3 = 10.34 \text{ GPa}$, $G_{12} = G_{13} = 6.895 \text{ GPa}$, $G_{13} = 6.205 \text{ GPa}$, $\nu_{12} = \nu_{13} = 0.22$, $\nu_{23} = 0.49$, $\rho = 1627 \text{ kg/m}^3$.
Geometric	$h_c / h = 0.73$, $a = 10h$, $R_{xt} = R_{xb} = R_{xc} = R_x = 0.67a$, $R_{yt} = R_{yb} = R_{yc} = R_y$, $a = b$.

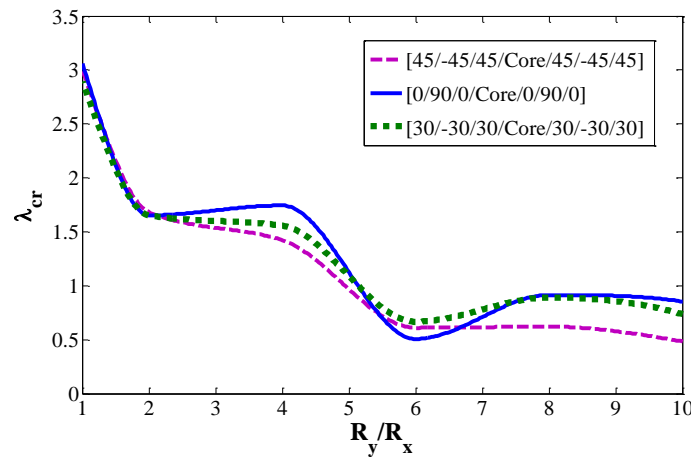


Fig. 2 Variation of dimensionless critical dynamic pressure with the radii curvatures ratio

composite sandwich panels with S.S. B.C.s is investigated. Mechanical and geometrical properties of a composite sandwich panel are given in Table 8. Cross ply [0/90/0/Core/0/90/0], angle ply [45/-45/-45/Core/45/-45/45] and [30/-30/30/Core/30/-30/30] stacking sequence are considered.

In Fig. 2, the variation of the dimensionless critical dynamic pressure ($\lambda_{cr} = \beta_a a^3 / D^{11}(0)$) with the radii curvatures ratio is presented. Fig. 2 shows that by increasing the radii curvatures ratio, the dimensionless critical dynamic pressures for three types of lay-ups are decreased. This behavior is predictable; because by increasing the radii curvatures ratio, the doubly curved panel is turned to a single curved panel and, since the bending stiffness of the spherical panels (doubly curved panels) is more than that of the cylindrical panels (single curved panels), the dimensionless critical dynamic pressure is decreased. For higher radii curvatures, the variation of the dimensionless critical dynamic pressure is insignificant.

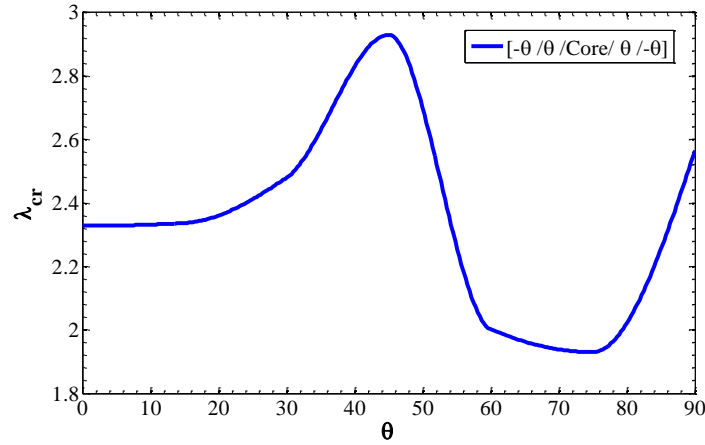


Fig. 3 Variation of dimensionless critical dynamic pressure with the fiber angle ($h_c/h_t=8$, $a=10h$, $R_{xt}=R_{xb}=R_{xc}=R_{yt}=R_{yb}=R_{yc}=0.67a$, $a=b$)

Example 6

In this example the effect of the fiber angle on the panel flutter of spherical composite sandwich panels with S.S. B.C.s is investigated. Mechanical properties of a composite sandwich panel are given in Table 8. The lay-up of the composite sandwich panel is $[-\theta/\theta/\text{Core}/\theta/-\theta]$.

In Fig. 3, the variation of the dimensionless critical dynamic pressure (λ_{cr}) with the fiber angle is presented. Fig. 3 demonstrates that, by increasing the fiber angle from 0 to 45, the dimensionless critical dynamic pressure and its increasing rate are increased; afterwards, by increasing the fiber angle from 45 to 75, the dimensionless critical dynamic pressure is decreased. Also, the highest critical dynamic pressure occurs at the angle ply panel ($\theta=45$).

Example 7

In this example the effect of type of varying thickness of the core on the panel flutter of doubly curved composite sandwich panels with S.S. B.C.s is investigated. To do this, change the curvature radii of the bottom face sheet to the curvature radii of the top face sheet ratio (R_b/R_t). Mechanical properties of a composite sandwich panel and stacking sequences are similar to Example 5.

In Fig. 4, the variation of the dimensionless critical dynamic pressure (λ_{cr}) with R_b/R_t ratio is presented. Fig. 4 shows that by increasing the R_b/R_t ratio, the dimensionless critical dynamic pressure fluctuation occurs. Also this figure demonstrates that the highest critical dynamic pressure for three types of lay-ups is occurred at the panel with R_b/R_t ratio -1. As shown in this figure, type of varying thickness of the core significantly affects the panel flutter response of doubly curved composite sandwich panels. As a result, modeling variable thickness doubly curved panels with doubly curved, single curved or flat panels with constant thicknesses cannot be accurately predicted the flutter behavior.

Example 8

In this example the effect of the temperature rise (ΔT) on the panel flutter of doubly curved composite sandwich panels with S.S. B.C.s is investigated. Mechanical properties of a composite sandwich panel are given in Table 8. Cross ply $[0/90/0/\text{Core}/0/90/0]$, angle ply $[45/-45/-45/\text{Core}/45/-45/45]$ and $[30/-30/30/\text{Core}/30/-30/30]$ stacking sequence are considered. In Fig. 5,

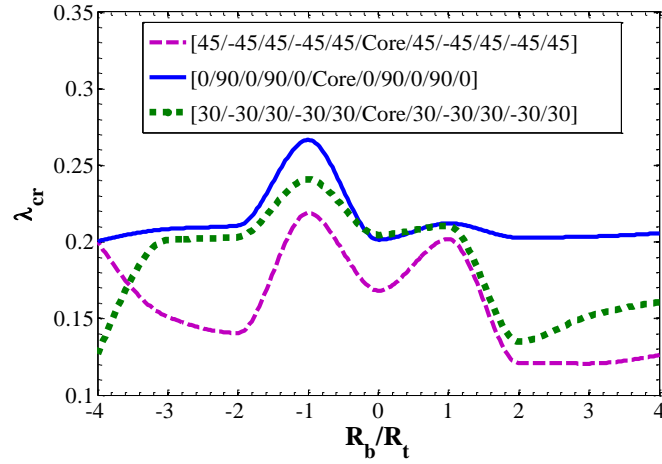


Fig. 4 Variation of dimensionless critical dynamic pressure with R_b/R_t ratio ($h_c/h=0.73$, $a=9h$, $R_{xt}=R_{yt}=R_t=a$, $R_{xb}=R_{yb}=R_b$)

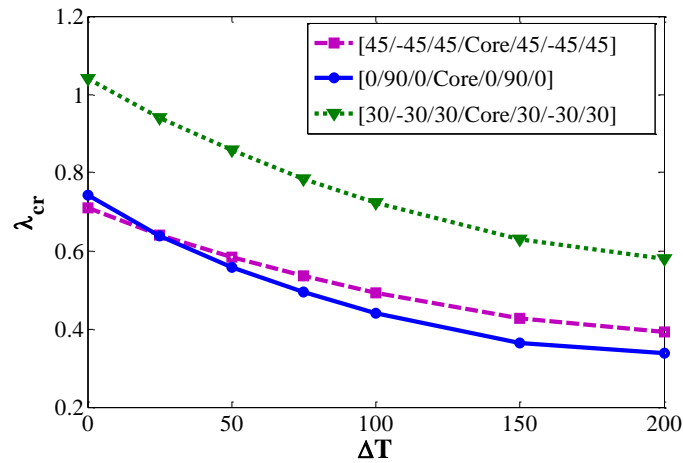


Fig. 5 Variation of dimensionless critical dynamic pressure with the temperature rise ($a=10\bar{h}$, $R_{xt}=R_{yt}=a$, $R_{xb}=R_{yb}=3a$)

the variation of the dimensionless critical dynamic pressure (λ_{cr}) with the temperature rise is presented. Fig. 5 shows that by increasing the temperature rise, the dimensionless critical dynamic pressure decreases.

Example 9

In this example the effect of the prestress on the panel flutter of spherical composite sandwich panels with S.S. B.C.s is investigated. Mechanical properties of a composite sandwich panel and stacking sequences are similar to Example 5.

In Table 9, the effect of the prestress ($N/N_{cr}=0, 0.2, 0.4, 0.6, 0.8$) on the dimensionless critical dynamic pressure (λ_{cr}) for different length to width ratio ($a/b=1,2,3$) is presented. Table 9 shows that by increasing the prestress, the dimensionless critical dynamic pressure for three types of lay-ups and all length to width ratio is decreased.

Table 9 Effect of prestress on the panel flutter of spherical composite sandwich panels $h_c/h=0.73$, $a=9h$, $R_{xt}=R_{xb}=R_{yt}=R_{yb}=R=a$

λ_{cr} ($N/N_{cr}=0.8$)	λ_{cr} ($N/N_{cr}=0.6$)	λ_{cr} ($N/N_{cr}=0.4$)	λ_{cr} ($N/N_{cr}=0.2$)	λ_{cr} ($N/N_{cr}=0$)	Lay-up type	a/b
0.6301	0.6789	0.7198	0.7566	0.7922	0/90/0	
0.5368	0.5846	0.6145	0.6419	0.6650	45/-45/45	1
0.5859	0.6351	0.6661	0.6937	0.7195	30/-30/30	
1.2933	1.3757	1.4478	1.5251	1.5878	0/90/0	
1.6601	1.7568	1.8389	1.9108	1.9602	45/-45/45	2
1.5398	1.6047	1.6815	1.7341	1.7928	30/-30/30	
1.3439	1.4348	1.5119	1.5769	1.6479	0/90/0	
1.3373	1.4036	1.4662	1.5176	1.5654	45/-45/45	3
1.3232	1.3948	1.4559	1.4981	1.5518	30/-30/30	
1.2645	1.3451	1.4220	1.4871	1.5487	0/90/0	
1.2569	1.3177	1.3903	1.4382	1.4907	45/-45/45	4
1.3094	1.3808	1.4421	1.4817	1.5389	30/-30/30	

5. Conclusions

In this work, the supersonic panel flutter of doubly curved composite sandwich panels with variable thickness under aerothermoelastic loading is studied based on a new improved higher order sandwich plate theory. The main conclusions are:

- The new higher-order sandwich panel theory used in this paper, can accurately predict the stability behavior of doubly curved composite sandwich panels.
- The highest flutter boundary is occurred at angle ply panels.
- With the increase of the radii curvatures ratio, the aeroelastic stability is decreased.
- Type of varying thicknesses of the core significantly affects the panel flutter response of doubly curved composite sandwich panels; as a result, modeling variable thickness doubly curved panels with constant thickness panels to predict flutter behavior of doubly curved panels is not strictly accurate.
- The highest critical dynamic pressure for variable thickness doubly curved panels is occurred at the panel with R_b/R_r ratio -1
- The aeroelastic stability decreases with the increase in temperature rise and in-plane stress.

References

Abbas, L.K., Rui, X., Marzocca, P., Abdalla, M. and De Breuker, R. (2011), "A parametric study on supersonic/hypersonic flutter behavior of aero-thermo-elastic geometrically imperfect curved skin panel", *Acta Mech.*, **222**, 41-57.

Armenakas, A.E., Gazis, D.C. and Herrmann, G. (1969), *Free Vibrations of Circular Cylindrical Shells*, Oxford, Pergamon Press.

Biglari, H. and Jafari, A.A. (2010), "Static and free vibration analyses of doubly curved composite sandwich panels with soft core based on a new three-layered mixed theory", *Proc. Inst. Mech. Eng., Part C: J.*

- Mech. Eng. Sci.*, **224**, 2332-2349.
- Fekrar., A., El Meiche, N., Bessaim, A., Tounsi, A. and Adda Bedia, E.A. (2012), "Buckling analysis of functionally graded hybrid composite plates using a new four variable refined plate theory", *Steel Comp. Struct.*, **13**(1), 91-107.
- Frostig, Y. and Baruch, M. (1994), "Free vibration of sandwich beams with a transversely flexible core: a high order approach", *J. Sound Vib.*, **176**(2), 195-208.
- Frostig, Y. and Thomsen, O.T. (2004), "Higher-order free vibration of sandwich panels with a flexible core", *Int. J. Solid. Struct.*, **41**, 1697-1724.
- Ganapathi, M. and Varadan, T.K. (1995), "Supersonic Flutter of laminated curved panels", *Defence Sci. J.*, **45**(2), 147-159.
- Jalili, S., Zamani, J., Shariyat, M., Jalili, N., Ajdari, M.A.B. and Jafari, M. (2014), "Experimental and numerical investigation of composite conical shells", *Struct. Eng. Mech.*, **49**(5), 555-568.
- Kheirikhah, M.M., Khalili, S.M.R. and Malekzadeh Fard, K. (2012), "Analytical solution for bending analysis of soft-core composite sandwich plates using improved high-order theory", *Struct. Eng. Mech.*, **44**(1), 15-34.
- Kuo, S.Y. (2011), "Flutter of rectangular composite plates with variable fiber pacing", *Comp. Struct.*, **93**, 2533-2540.
- Leissa, A.W. and Kadi, A.S. (1971), "Curvature effects on shallow shell vibrations", *J. Sound Vib.*, **16**(2), 173-187.
- Li, F.M. and Song, Z.G. (2013), "Flutter and thermal buckling control for composite laminated panels in supersonic flow", *J. Sound Vib.*, **332**, 5678-5695.
- Malekzadefard, K., Livani, M. and Ashena Ghasemi, F. (2014a), "Improved high order free vibration analysis of thick double curved sandwich panels with transversely flexible cores", *Lat. Am. J. Solid. Struct.*, **11**, 2284-2307.
- Malekzadefard, K., Livani, M., Veisi, A. and Gholami, M. (2014b), "Improved high-order bending analysis of double curved sandwich panels subjected to multiple loading conditions", *Lat. Am. J. Solid. Struct.*, **11**, 1591-1614.
- Malekzadeh Fard, K. and Livani, M. (2015), "The buckling of truncated conical sandwich panels under axial compression and external pressure", *Proc. Inst. Mech. Eng., Part C: J. Mech. Eng. Sci.*, **229**(11), 1965-1978.
- Meunier, M. and Sheno, R.A. (1999), "Free vibration analysis of composite sandwich plates", *Proc. Inst. Mech. Eng., Part C: J. Mech. Eng. Sci.*, **213**(7), 715-727.
- Moradi, S. and Mansouri, M.H. (2012), "Thermal buckling analysis of shear deformable laminated orthotropic plates by differential quadrature", *Steel Compos. Struct.*, **12**(2), 129-147.
- Naj, R., Sabzikar Boroujerdy, M. and Eslami, M.R. (2008), "Thermal and mechanical instability of functionally graded truncated conical shells", *Thin Wall. Struct.*, **46**(1), 65-78.
- Navazi, H.M. and Haddadpour, H. (2007), "Aero-thermoelastic stability of functionally graded plates", *Compos. Struct.*, **80**, 580-587.
- Navazi, H.M. and Haddadpour, H. (2011), "Nonlinear aero-thermoelastic analysis of homogeneous and functionally graded plates in supersonic airflow using coupled models", *Compos. Struct.*, **93**, 2554-2565.
- Nguyen, T.K., Thai, H.T. and Vo, P.T. (2015), "A refined higher-order shear deformation theory for bending, vibration and buckling analysis of functionally graded sandwich plates", *Steel Compos. Struct.*, **18**(1), 91-120.
- Nguyen, T.K., Vo, P.T. and Thai, H.T. (2014a), "Vibration and buckling analysis of functionally graded sandwich plates with improved transverse shear stiffness based on the first-order shear deformation theory", *Proc. Inst. Mech. Eng., Part C: J. Mech. Eng. Sci.*, **228**(12), 2110-2131.
- Nguyen, V.H., Nguyen, T.K., Thai, H.T. and Vo, T.P. (2014b), "A new inverse trigonometric shear deformation theory for isotropic and functionally graded sandwich plates", *Compos. Part B: Eng.*, **66**, 233-246.
- Rahmani, O., Khalili, S.M.R. and Malekzadeh, K. (2009), "Free vibration response of composite sandwich cylindrical shell with flexible core", *Compos. Struct.*, **92**, 1269-1281.

- Rahmani, O., Khalili, S.M.R. and Malekzadeh, K. (2010), "Free vibration response of composite sandwich cylindrical shell with flexible core", *Compos. Struct.*, **92**, 1269-1281.
- Reddy, J.N. (2004), *Mechanics of Laminated Composite Plates and Shells, Theory and Analysis*. CRC Press, New York, USA.
- Rezaiee-Pajand, M., Shahabian, F. and Tavakoli, F.H. (2012), "A new higher-order triangular plate bending element for the analysis of laminated composite and sandwich plates", *Struct. Eng. Mech.*, **43**(2), 253-271.
- Sankar, A., Natarajan, S., Ben Zineb, T. and Ganapathi, M. (2015), "Investigation of supersonic flutter of thick doubly curved sandwich panels with CNT reinforced facesheets using higher-order structural theory", *Compos. Struct.*, **127**, 340-355.
- Sankar, A., Natarajan, S., Haboussi, M., Ramajeyathilagam, K. and Ganapathi, M. (2014), "Panel flutter characteristics of sandwich plates with CNT reinforced facesheets using an accurate higher-order theory", *J. Fluid. Struct.*, **50**, 376-391.
- Sawyer, J.W. (1977), "Flutter and buckling of general laminated plates", *J. Aircraft*, **14**, 387-393.
- Seresta, O. (2007), "Buckling, flutter, and postbuckling optimization of composite structures", PHD Thesis, Aerospace Engineering, Virginia Polytechnic Institute and State University.
- Shiau, L.C., Kuo, S.Y. and Liu, Y.P. (2012), "Aerothermoelastic analysis of composite laminated plates", *Compos. Struct.*, **94**, 1982-1990.
- Shin, W.H., Oh, I.K. and Lee, I. (2009), "Nonlinear flutter of aerothermally buckled composite shells with damping treatments", *J. Sound Vib.*, **324**, 556-569.
- Sohn, K.J. and Kim, J.H. (2009), "Nonlinear thermal flutter of functionally graded panels under a supersonic flow", *Compos. Struct.*, **88**, 380-387.
- Song, Z.G. and Li, F.M. (2014), "Aeroelastic analysis and active flutter control of nonlinear lattice sandwich beam", *Nonlin. Dyn.*, **76**(1), 57-68.
- Song, Z.G. and Li, F.M. (2016), "Aerothermoelastic analysis of lattice sandwich composite panels in supersonic airflow", *Meccanica*, **51**(4), 877-891.
- Thai, H.T., Nguyen, T.K., Vo, T.P. and Lee, J. (2014), "Analysis of functionally graded sandwich plates using a new first-order shear deformation theory", *Eur. J. Mech. A/Solid.*, **45**, 211-225.
- Wang, Q. (2003), "On complex flutter and buckling analysis of a beam structure subjected to static follower force", *Struct. Eng. Mech.*, **16**(5), 533-556.
- Yang, Z., Zhou, J. and Gu, Y. (2014), "Integrated analysis on static dynamic aeroelasticity of curved panels based on a modified local piston theory", *J. Sound Vib.*, **333**, 5885-5897.
- Zhao, M.H. and Zhang, W. (2014), "Nonlinear dynamics of composite laminated cantilever rectangular plate subject to third-order piston aerodynamics", *Acta Mech.*, **225**, 1985-2004.
- Zhong, C. and Reimerdes, H.G. (2007), "Stability behavior of cylindrical and conical sandwich shells with flexible core", *J. Sand. Struct. Mater.*, **9**, 143-166.